

Effect of Variable Viscosity on Entropy Generation Analysis Due to Graphene Oxide Nanofluid Convective Flow in Concentric Cylinders

Jagadeeshwar Pashikanti^{1,*}, D. R. Susmitha Priyadharshini¹, and Ali J. Chamkha²

¹Department of Science and Humanities, Indian Institute of Information Technology Tiruchirappalli, Tiruchirappalli, Tamil Nadu 620012, India

²Kuwait College of Science and Technology (KCST), 7th Ring Road, Doha District, 35004, Kuwait

Aggregated studies of graphene nanoparticles is important for the effective utilization of their striking thermo-physical properties and extensive industrial applications. This investigation is one such computational study to explore the flow of graphene oxide nanofluids with temperature dependant viscosity between two concentric cylinders. Buongiorno model is used to develop the flow of graphene nanofluids including the impacts of Soret and Dufour effects and the effects of nanoparticle characteristics such as thermophoresis and Brownian motion. The modelled equations are transformed and are numerically solved using linearization method together with Chebyshev's spectral collocation method under convective conditions. The impacts of embedded parameters on temperature, concentration and skin friction profiles of the chosen nanofluid and their consequent impacts on the predominant cause for the generated entropy are studied. From the tabulated values of Nusselt number and Sherwood number, it is observed that convective heat transfer can be enhanced by thermal Biot number whereas Soret number enhances diffusive mass transfer and variable viscosity parameter preferably reduces the skin friction. A comparison table is presented and it shows that the values obtained from the present method are in good agreement with existing literature. Also, the obtained results are depicted and interpreted in detail. Furthermore, entropy generation is analysed and its irreversibility is calculated.

KEYWORDS: Graphene Nanofluids, Buongiorno Model, Entropy Generation.

1. INTRODUCTION

Nanofluids are preferable for their efficiency compared to conventional viscous fluids and microfluids. Unlike other fluids with larger dispersed particles, they are devoid of deposition, clogging and erosion of flow channels, besides their striking heat transfer enhancement. Suggestions from literature showed that the nanoparticles could develop slip velocity from various attributes. But, Buongiorno in 2006,¹ documented that the slip mechanisms are insignificant in turbulence, except, when the particles are carried by turbulent eddies. Our focus is on laminar flow where, thermophoresis and Brownian motion are the only two influential slip mechanisms. The other mechanisms such as gravity settling, fluid drainage, Magnus effect and diffusiophoresis can be neglected. Besides, the advantages of nanofluids on the whole, the nanoparticles dispersed in

the fluids greatly influences the behaviour of the nanofluids. In view of the thermophysical properties, graphene nanoparticles are an excellent choice for an enhanced thermal performance. Graphene is a two-dimensional structure of carbon atoms derived from naturally occurring graphite which is obtained as crystalline carbon. For its, striking heat transfer enhancement and thermal conductivity, it is marginally used by researchers in their studies. Some of the applications of graphene based nanofluids include their uses in lithium-ion batteries, biosensors, supercapacitors, medical suspensions etc.

Classical studies on fluid flow between concentric cylinders such as the study on two dimensional natural convection for low Rayleigh numbers by Mack and Bishop² and stability analysis of Couette flow by Renardy³ have paved the ways for further exploration of the geometry. The flow in concentric cylinders have numerous practical applications such as viscometers, rheometers, mixing devices such as Taylor-Couette reactors etc. Some of the other computational studies on water based nanofluid flow between concentric cylinders to be noted are the natural convection of water based aluminium oxide, silver,

*Author to whom correspondence should be addressed.

Emails: jagadeeshwar.pashikanti@gmail.com,
jagadeeshwar@iiitt.ac.in

Received: 18 May 2023

Accepted: 24 August 2023

copper and titanium oxide nanofluids in an annulus is studied by Abu-Nada and Hijazi.⁴ From the conclusions, it is established that, near the inner cylinder, for larger Rayleigh numbers, alumina nanofluid enhances convective heat transfer whereas for lower values, the Nusselt number is enhanced. The study conducted by Yu et al.⁵ investigates the water based copper oxide particles for four different volume fractions and concludes that the time-averaged Nusselt number decreases with volume fraction. Abedini and Emadoddin⁶ investigated the mixed convection of water based titanium oxide, copper, aluminium oxide and silver nanofluids in an annulus. In this study, the results show that increasing the Richardson number and Rayleigh number enhances the Nusselt number. The convection of copper nanofluids in water is studied numerically by Liu et al.⁷ with porous medium in two geometries and is inferred to enhance the Nusselt number with porosity in both the geometries. Recently, Gouran et al.⁸ presented an examination on MHD (magnetohydrodynamic) flow in concentric cylinders with a conclusion that the temperature profiles decrease with Hartmann number and radiation parameter whereas Nusselt number increases. Pordanjani and Aghakhani⁹ presented a numerical examination of alumina nanofluid flow in an inclined channel of concentric cylinders under the influence of magnetic field with an inferred enhancement in conductive heat transfer.

Commonly, the fluid flows are computationally investigated with constant fluid properties like constant viscosity and constant thermal conductivity, in view of calculative convenience. But, practically these fluid properties tend to vary with temperature, for example, in flow fields with non-uniform temperature distributions, fluid viscosity varies noticeably. Hence, it is important to consider the variabilities to accurately study the mechanisms of heat transfer. Lai and Kulacki¹⁰ were the first to report the impacts of temperature dependant viscosity and porous media due to the fluid flowing over a plate. Eyring-Powell fluid flow over a stretching cylinder assuming the viscosity to be linearly dependant on temperature is examined by Malik et al.¹¹ Hussain and Ullah¹² analytically studied Walter's B fluid flow with variable viscosity along a stretching cylinder. Kaladhar et al.¹³ studied the Joule heating effects of the flow in a vertical channel with porous medium. Srinivasacharya and Jagadeeshwar¹⁴ numerically examined the MHD flow with temperature dependant thermal conductivity and viscosity over a sheet stretching exponentially. They¹⁵ further extended the study on the effects of Joule heating in an exponentially stretching sheet. Irfan et al.¹⁶ numerically investigated the fluid flows with constant as well as variable properties along a sheet whose thickness varies, where the numerical analysis is conducted using a simplified finite difference method (SFDM).

By Fourier's and Fick's laws, cross diffusion effects acquire trivial importance in heat and mass transfer investigations, because of their negligible contribution. But, in

fluid flows, the energy fluxes are complexly related with riding potentials and are associated with temperature and concentration gradients. Such heat flux due to concentration gradient is called the Dufour effect whereas mass flux due to thermal gradient is Soret effect. In academic branches such as geosciences, hydrology, petrology, aerodynamics etc., these cross-diffusion effects strengthen and hence are irresistible to ignore as acknowledged by Eckert and Drake.¹⁷ Computational studies on the flow of fluids with cross-diffusion effects and varying properties such as the study reporting the impacts of temperature dependant thermal conductivity and temperature dependant viscosity due to the nanofluid flow over a wavy surface is investigated by Srinivasacharya et al.¹⁸ The fluid flow between two rotating discs with cross-diffusion effects were modelled and analytically solved by Shah et al.¹⁹ Rehman and Salleh²⁰ studied the flow of graphene oxide nanofluids with water and ethylene glycol as basefluids of varying thermal conductivity over a linearly stretching surface. Srinivasacharya and Jagadeeshwar²¹ conducted a study on viscous fluids with constant electrical conductivity along a stretching sheet under Hall current and cross-diffusion effects. Casson nanofluid flow with variable properties in non-Darcian porous medium with slip and convective conditions is examined by Gbadeyan et al.²² Sharma et al.²³ presented a numerical and statistical investigation on Joule dissipation effect due to Maxwell nanofluid with dispersed graphene nanoparticles flowing past a stretching sheet.

Some notable computational studies on nanofluids include, the study of slip flow and radiative heat transfer behavior of Titanium alloy and ferromagnetic nanoparticles along with suspension of dusty fluid by Souayeh et al.²⁴ Reddy et al.²⁵ focused on the two dimensional flow of an incompressible hybrid dusty fluid through a Darcy-Forchheimer medium over a stretched sheet. Reddy et al.²⁶ investigated the magnetohydrodynamic flow and heat transfer of water based molybdenum disulfide and ferro sulfate hybrid nanofluid over a rotating disk by considering the Arrhenius activation energy. Kumar et al.²⁷ conducted a stability analysis of heat transfer enhancement occurring due to the influence of significant properties variation of fluids in the presence of solar radiation with ferromagnetic hybrid nanofluids. Ganesh Kumar²⁸ conducted a stream line analysis on aluminium alloys over a stretching sheet in the presence of radially varying magnetic dipole field using Koo and Kleinstreuer model. Naik et al.²⁹ conducted a bidirectional investigation of the effect of activation energy on carbonized fluid flow and radiative heat transfer across a stretched surface. Prakasha et al.³⁰ studies the impacts of a magnetic dipole on swirling flow and radiative heat transmission of water based alumina nanofluids over a deformable cylinder. Sudharani et al.³¹ proposed a novel mathematical model for improving heat transfer using trihybrid nanofluids by investigating the slip flow and radiative heat transfer over a moving sheet with polymer-based tri hybrid nanofluid.

Furthermore, graphene has the highest thermal conductivity of all the known materials. For its advantageous thermophysical, mechanical and chemical properties, its immense use as coolants is raising aloft. The contribution to renewable energy reassures economically large scale practical applications in view of power storage and capacity. Such significance interests us in computationally studying graphene based nanofluid flow in several geometries. Henceforth, limited applied and computational studies demands the attention of applied mathematicians and engineers for further investigations of graphene based nanofluids in different geometries. Also, variable thermo-physical properties has industrial applications such as manufacturing of dyes, fertilizers and polymers etc. In spite of all the computational studies on the geometry of concentric cylinders, literature lacks the convective study of graphene oxide nanofluid flow with combined cross-diffusion effects in concentric cylinders. The aim of this paper is to bridge such a gap by modelling and analysing the flow of water based graphene oxide nanofluid with temperature dependant viscosity, between two concentric cylinders, thereby contributing to the model and parameter analyses of flows in concentric cylinders such as spacecrafts, turbines, atomic plants, missiles, satellites etc. The modelled equations are numerically solved and the values are graphically represented.

2. GOVERNING EQUATIONS

Two vertically aligned infinite concentric cylinders are considered with radii a and b such that ($b > a$) and the outer cylinder is assumed to rotate with an angular velocity Ω . Any fluid particle in the flow is represented by the cylindrical coordinates (r, Θ, z) . Graphene oxide nanofluid flows between the cylinders with a tangential velocity u and constant pressure gradient $\partial P/\partial \Theta$. The flow is assumed to be fully developed and axisymmetric. The variable nanofluid viscosity is given by $1/\mu_{bf} = b(T - T_r)$, where the constants $b = \delta/\mu_\infty$ and $T_r = T_\infty - 1/\delta$ are dependant on the thermal property of the fluid δ and the reference state. A constant heat source Q_0 introduced. The body forces due to gravity, Soret and Dufour effects, the effects caused by characteristic nanoparticle phenomena namely thermophoresis and Brownian motion are considered. The schematic representation of the flow is given in Figure 1.

Considering the body force due to gravity, cross-diffusion effects and the effects caused by characteristic nanoparticles phenomena namely Brownian motion and thermophoresis and adapting the nanofluid model,¹ the appropriate governing equations at the boundary layer are given by

$$\frac{\partial u}{\partial \Theta} = 0 \quad (1)$$

$$\frac{\rho_{nf} u^2}{r} = \frac{\partial p}{\partial r} \quad (2)$$

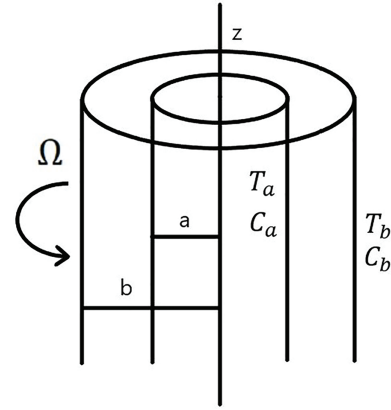


Fig. 1. Schematic representation of the flow in concentric cylinders.

$$\begin{aligned} & \mu_{nf} \left(\frac{\partial^2 u}{\partial r^2} + \frac{\partial \mu_{nf}}{\partial r} \left(\frac{\partial u}{\partial r} \right) + \frac{1}{r} \frac{\partial u}{\partial r} - \frac{u}{r^2} \right) \\ & + (1 - C_a)(T - T_a)g(\rho\beta)_{nf} - (\rho_p - \rho_{bf}) \\ & \times (C - C_a)g - \frac{1}{r} \frac{\partial p}{\partial \Theta} = 0 \end{aligned} \quad (3)$$

$$\begin{aligned} & \frac{\kappa_{nf}}{(\rho C_p)_{nf}} \left(\frac{\partial^2 T}{\partial r^2} + \frac{1}{r} \frac{\partial T}{\partial r} \right) + \tau \left(D_B \left(\frac{\partial T}{\partial r} \frac{\partial C}{\partial r} \right) + \frac{D_T}{T_a} \left(\frac{\partial T}{\partial r} \right)^2 \right) \\ & + \frac{D_B K_T \rho_{nf}}{(\rho C_p)_{nf} C_s} \left(\frac{\partial^2 C}{\partial r^2} + \frac{1}{r} \frac{\partial C}{\partial r} \right) + \frac{Q_0}{(\rho C_p)_{nf}} (T - T_a) = 0 \end{aligned} \quad (4)$$

$$\begin{aligned} & D_B \left(\frac{\partial^2 C}{\partial r^2} + \frac{1}{r} \frac{\partial C}{\partial r} \right) + \frac{D_T}{T_a} \left(\frac{\partial^2 T}{\partial r^2} + \frac{1}{r} \frac{\partial T}{\partial r} \right) \\ & + \frac{D_T K_T}{T_a} \left(\frac{\partial^2 T}{\partial r^2} + \frac{1}{r} \frac{\partial T}{\partial r} \right) = 0 \end{aligned} \quad (5)$$

The corresponding convective no-slip boundary conditions are¹⁸

$$\left. \begin{aligned} & \text{at } r = a, \quad u = 0, \quad -\kappa_{nf} \frac{\partial T}{\partial r} = h(T_a - T), \\ & -D_m \frac{\partial C}{\partial r} = k_m(C_a - C) \\ & \text{at } r = b, \quad u = b\Omega, \quad -\kappa_{nf} \frac{\partial T}{\partial r} = h(T - T_b), \\ & -D_m \frac{\partial C}{\partial r} = k_m(C - C_b) \end{aligned} \right\} \quad (6)$$

The notations T_a and T_b indicate the fluid temperatures at the inner and outer cylinders respectively, and similarly C_a and C_b are nanofluid concentrations at the inner and outer cylinders, K_T , C_s , h and k_m are the thermal diffusion ratio, concentration susceptibility, coefficients of heat transfer and mass transfer and κ denotes thermal conductivity and D_m mass diffusivity.

The thermophysical properties of nanofluids defined in Refs. [36, 37] are taken as

$$\begin{aligned} \mu_{nf} &= \frac{\mu_{bf}}{(1 - \Phi)^{2.5}}, \quad \rho_{nf} = (1 - \Phi)\rho_{bf} + \Phi\rho_{sp}, \\ \alpha_{nf} &= \frac{\kappa_{nf}}{(\rho C_p)_{nf}}, \quad \frac{\kappa_{nf}}{\kappa_{bf}} = \frac{\kappa_{sp} + 2\kappa_{bf} + 2\Phi(\kappa_{bf} - \kappa_{sp})}{\kappa_{sp} + 2\kappa_{bf} - \Phi(\kappa_{bf} - \kappa_{sp})}, \\ (\rho C_p)_{nf} &= (1 - \Phi)(\rho C_p)_{bf} + \Phi(\rho C_p)_{sp}, \\ (\rho\beta)_{nf} &= (1 - \Phi)(\rho\beta)_{bf} + \Phi(\rho\beta)_{sp}, \end{aligned}$$

The suffixes *bf*, *nf*, *sp* denote base fluid, nanofluid and solid particle and the quantities μ , ρ , C_p , α , β and κ denote dynamic viscosity, density, specific heat capacity, thermal diffusivity, thermal expansion coefficient and thermal conductivity respectively. The values of thermophysical properties of water and graphene oxide are presented in Table I.

The similarity variables used for transformation can be defined as follows:

$$\left. \begin{aligned} \eta &= \frac{r^2}{b^2}, \quad u = \frac{\Omega}{\sqrt{\eta}} f(\eta), \quad \theta(\eta) = \frac{T - T_a}{T_f - T_a}, \\ \phi(\eta) &= \frac{C - C_a}{C_f - C_a}, \quad P = \frac{pb}{\Omega\mu_\infty} \end{aligned} \right\} \quad (7)$$

Using these variables, the equations (1)–(6) are written as the given ordinary differential equations.

$$4\eta f'' \left(1 - \frac{\theta}{\Theta_r}\right) + \frac{1}{\Theta_r} 4\eta \left(f' - \frac{f}{\eta}\right) \theta' + A_1 \frac{Gr}{Re} \sqrt{\eta} \times \left(1 - \frac{\theta}{\Theta_r}\right) (A_2 \theta - Nr \phi) - A_1 P_1 \left(1 - \frac{\theta}{\Theta_r}\right)^2 = 0 \quad (8)$$

$$\eta \theta'' + \theta' + A_3 A_4 \eta \theta' (N_b \phi' + N_t \theta') + A_3 A_5 Du (\eta \phi'' + \phi') + A_3 Pr q_1 \theta = 0 \quad (9)$$

$$\eta \phi'' + \phi' + \left(\frac{N_t}{N_b} + Sr\right) (\eta \theta'' + \theta') = 0 \quad (10)$$

The corresponding transformed boundary conditions are written as

$$\left. \begin{aligned} \text{at } \eta = \eta_0 &= \frac{a^2}{b^2}, \quad f = 0, \quad 2\sqrt{\eta_0} \theta' = A_3 Bi_t \theta, \\ 2\sqrt{\eta_0} \phi' &= Bi_c (1 - \phi) \\ \text{at } \eta = 1, \quad f &= 1, \\ 2\theta' &= A_3 Bi_t (1 - \theta), \quad 2\phi' = Bi_c (1 - \phi) \end{aligned} \right\} \quad (11)$$

The constant coefficients and the nondimensional numbers used, namely, the Grashof number Gr , Reynolds number Re , buoyancy ratio N_r , constant pressure gradient P_1 , heat source parameter q_1 , variable viscosity parameter Θ_r ,

thermophoresis parameter N_t , Soret number Sr , Brownian motion parameter N_b , Dufour number Du , Schmidt number Sc , thermal diffusivity α_{nf} , thermal and concentration Biot number Bi_t and Bi_c and heat capacity ratio τ are defined as

$$\begin{aligned} A_1 &= (1 - \Phi)^{2.5}, \quad A_2 = 1 - \Phi + \Phi \frac{(\rho\beta)_{sp}}{(\rho\beta)_{bf}}, \quad A_3 = \frac{\kappa_{bf}}{\kappa_{nf}}, \\ A_4 &= 1 - \Phi + \Phi \frac{(\rho C_p)_{sp}}{(\rho C_p)_{bf}}, \quad A_5 = 1 - \Phi + \Phi \frac{\rho_{sp}}{\rho_{bf}}, \\ Gr &= \frac{\rho_{bf}^2 g \beta (T_b - T_a) (1 - C_a) b^3}{\mu_\infty^2}, \quad Re = \frac{\rho_{bf} \Omega b}{\mu_\infty}, \\ N_r &= \frac{(\rho_p - \rho_{bf})(C_b - C_a)}{(\rho\beta)_{bf} (1 - C_a) (T_b - T_a)}, \quad N_b = \frac{\tau D_B (C_b - C_a)}{\alpha_{nf}}, \\ N_t &= \frac{\tau D_T (T_b - T_a)}{T_a \alpha_{nf}}, \quad Bi_t = \frac{hb}{\kappa_{bf}}, \quad Bi_c = \frac{k_m b}{D_m}, \\ \tau &= \frac{(\rho C_p)_{sp}}{(\rho C_p)_{nf}}, \quad P_1 = \frac{1}{\mu_\infty \Omega} \frac{\partial p}{\partial \theta}, \quad \alpha = \frac{\kappa_{bf}}{(\rho C P)_{bf}}, \\ q_1 &= \frac{Q_0 b^2}{4\mu_\infty C_{pbf}}, \quad Du = \frac{D_B K_T (C_b - C_a)}{C_{pbf} C_s (T_b - T_a)}, \\ Sr &= \frac{D_T K_T (T_b - T_a)}{D_B T_a (C_b - C_a)}, \quad Pr_\infty = \frac{\mu_\infty C_{pbf}}{\kappa_{bf}} \end{aligned}$$

The variable viscosity parameter is $\Theta_r = -1/(\delta(T_b - T_a))$, by definition, and by using appropriate simplifications, it is written as $\Theta_r = T_r - T_a/T_b - T_a$. It is notable that, as $\Theta_r \rightarrow \infty$, variable viscosity behaves as a constant ($\mu_{bf} = \mu_\infty$) and hence the Prandtl number behaves as constant ($Pr = Pr_\infty$).

The numbers of practical importance namely local Nusselt number Nu_z , local Sherwood number Sh_z and skin friction C_f are derived as

$$\begin{aligned} \frac{Nu_\eta}{2} &= -\theta'(\eta), \quad \frac{Sh_\eta}{2} = -\phi'(\eta), \\ \eta C_f Re_\eta &= A_6 \left(1 - \frac{\theta}{\Theta_r}\right)^{-1} (\eta f'(\eta) - f(\eta)) \end{aligned} \quad (12)$$

$$\text{at } \eta = \eta_0 \quad \text{and} \quad \eta = 1$$

where $A_6 = 4(1 - \Phi)^{-2.5} (1 - \Phi + \Phi(\rho_{sp}/\rho_{bf}))^{-1}$ is a constant. We propose an assessment for the generated entropy and derive the entropy generation number, in the next section.

Table I. Values of thermophysical properties^{32–35}

Property (Units)	Water	Graphene oxide
ρ (kg/m ³)	997.1	1800
C_p (J/kg K)	4179	717
κ (W/mK)	0.613	5000
β (10 ⁻⁵ /K)	21	28.4

3. ENTROPY GENERATION ANALYSIS

The generated entropy depends on three parts namely, the entropy generated due to temperature term, the entropy caused by viscous dissipation term and that due to concentration term. Hence the entropy generation rate, S_G can be written as³⁸

$$S_G = \frac{\kappa_{nf}}{T_a^2} \left(\frac{\partial T}{\partial r} \right)^2 + \frac{\mu_{nf}}{T_a} \left(\frac{\partial u}{\partial r} - \frac{u}{r} \right)^2 + RD_B \left(\frac{\partial C}{\partial r} \right) \times \left(\frac{1}{C_a} \left(\frac{\partial C}{\partial r} \right) + \frac{1}{T_a} \left(\frac{\partial T}{\partial r} \right) \right) \quad (13)$$

where the first term on the RHS gives the thermodynamic irreversibility induced by temperature, the next term is the irreversibility induced by viscous dissipation whereas the last term is ascribed to concentration. The characteristic entropy generation rate S_{G_0} , is given by $S_{G_0} = \kappa_{nf}(T_b - T_a)^2 / (T_a L)^2$. From S_G and S_{G_0} , the dimensionless entropy generation number is given by

$$N_S = \frac{S_G}{S_{G_0}} \quad (14)$$

Using the similarity variables, the N_S can also be written as

$$\left(1 - \frac{\theta}{\Theta_r} \right)^2 \eta^2 N_S = \frac{4}{\chi} \left(\left(1 - \frac{\theta}{\Theta_r} \right)^2 \eta^3 \theta'^2 + \frac{A_3 Ec Pr_\infty}{A_1 \Omega_T} \times \left(1 - \frac{\theta}{\Theta_r} \right) (\eta f' - f)^2 + \left(1 - \frac{\theta}{\Theta_r} \right) \times \frac{A_3 M_m \Omega_C \eta^3}{\chi \Omega_T} \phi' \left(\frac{\Omega_C}{\Omega_T} \phi' + \theta' \right) \right) \quad (15)$$

$$= N_{S_h} + N_{S_f} + N_{S_m} \quad (16)$$

where N_{S_h} is the irreversibility by heat transfer, N_{S_f} is the irreversibility by fluid friction and N_{S_m} is the irreversibility caused by mass transfer. The nondimensional parameters in (15) are defined as Eckert number $Ec = \Omega^2 / (C_{p_{bf}}(T_b - T_a))$, constant parameter $\chi = d^2 / L^2$, temperature parameter $\Omega_T = (T_b - T_a) / T_a$, concentration parameter $\Omega_C = (C_b - C_a) / C_a$ and the combined heat and mass transfer parameter $M_m = RD_B C_a / \kappa_{bf}$.

The predominant cause for entropy generation is determined from Bejan number, $Be = N_{S_h} / N_S$. Eliciting from the entropy distribution ratio given by Bejan,³⁹ Poeletti et al.⁴⁰ proposed if $Be > 0.5$, then the irreversibility influenced by heat transfer is the major cause of entropy generation, if $Be < 0.5$, then the entropy generation is influenced by fluid friction and mass transfer irreversibilities and if $Be = 0.5$, then contribution to the generated entropy comes equally from all the three irreversibilities namely, fluid friction, heat transfer and mass transfer.

4. NUMERICAL SOLUTION

The Spectral quasilinearization method (SQLM)^{18,41,42} is adapted to solve the ODEs (8)–(10) and the associated

boundary conditions (11). We linearize the nonlinear terms by using Taylor series expansion. Let f_r , θ_r and ϕ_r be the solution of the differential equations. Then, assuming f_{r+1} , θ_{r+1} and ϕ_{r+1} to be the improved solutions, the ODEs are solved. By expanding the nonlinear terms using Taylor series expansion about the solution and neglecting higher order derivatives, the following linearized equations are obtained:

$$a_{1,r} f''_{r+1} + a_{2,r} f'_{r+1} + a_{3,r} f_{r+1} + a_{4,r} \theta_{r+1} + a_{5,r} \theta'_{r+1} + a_{6,r} \phi_{r+1} = p_r \quad (17)$$

$$b_{1,r} \theta''_{r+1} + b_{2,r} \theta'_{r+1} + b_{3,r} \theta_{r+1} + b_{4,r} \phi'_{r+1} + b_{5,r} \phi_{r+1} = q_r \quad (18)$$

$$c_{1,r} \phi''_{r+1} + c_{2,r} \phi'_{r+1} + c_{3,r} \phi_{r+1} + \phi_{r+1} = 0 \quad (19)$$

The corresponding boundary conditions are,

$$\begin{aligned} \text{at } \eta = \eta_0, \quad f_{r+1} = 0, \quad 2\sqrt{\eta_0} \theta'_{r+1} = \theta_{r+1} A_3 Bi_t, \\ 2\sqrt{\eta_0} \phi'_{r+1} = Bi_c (1 - \phi_{r+1}) \\ \text{at } \eta = 1, \quad f_{r+1} = 1, \quad 2\theta'_{r+1} = A_3 Bi_t (1 - \theta_{r+1}), \\ 2\phi'_{r+1} = Bi_c (1 - \phi_{r+1}) \end{aligned} \quad (20)$$

The coefficients in the above equations are given by

$$\begin{aligned} a_{1,r} &= 4\eta \left(1 - \frac{\theta_r}{\Theta_r} \right), \quad a_{2,r} = \frac{4\eta}{\Theta_r} \theta'_r, \\ a_{3,r} &= \frac{-4}{\Theta_r} \theta'_r, \quad a_{4,r} = \frac{4}{\Theta_r} \eta (f'_r - f_r) \\ a_{5,r} &= \frac{-4\eta}{\Theta_r} f''_r + \frac{Gr}{Re} \sqrt{\eta} A_1 \left(A_2 \left(1 + 3 \frac{3\theta_r^2}{\Theta_r^2} - \frac{4\theta_r}{\Theta_r} \right) \right. \\ &\quad \left. - N_r \left(\frac{2\theta_r \phi_r}{\Theta_r^2} - \frac{2\phi_r}{\Theta_r} \right) \right) + A_1 P_1 \left(\frac{2}{\Theta_r} - \frac{2\theta_r}{\Theta_r^2} \right) \\ a_{6,r} &= \frac{Gr}{Re} \sqrt{\eta} A_1 N_r \left(1 - \frac{\theta_r^2}{\Theta_r} - \frac{2\theta_r}{\Theta_r} \right), \quad b_{1,r} = \eta, \\ b_{2,r} &= 1 + A_3 A_4 \eta (N_b \phi'_r + 2N_t \theta'_r), \quad b_{3,r} = A_3 Pr q_1 \end{aligned}$$

Table II. Comparison of $f(\eta)$ values calculated by the present method for $Gr = P_1 = R_d = C_R = 0$.

η	Present study	Sinha and Chaudhary ⁴⁵
1	1	1
0.98165	0.975528	0.97546
0.92838	0.904509	0.90453
0.84542	0.793894	0.79386
0.74088	0.654510	0.65453
0.625	0.500003	0.5
0.50912	0.345494	0.34546
0.40458	0.206110	0.20613
0.32162	0.095493	0.09546
0.26835	0.024472	0.02453
0.25	0	0

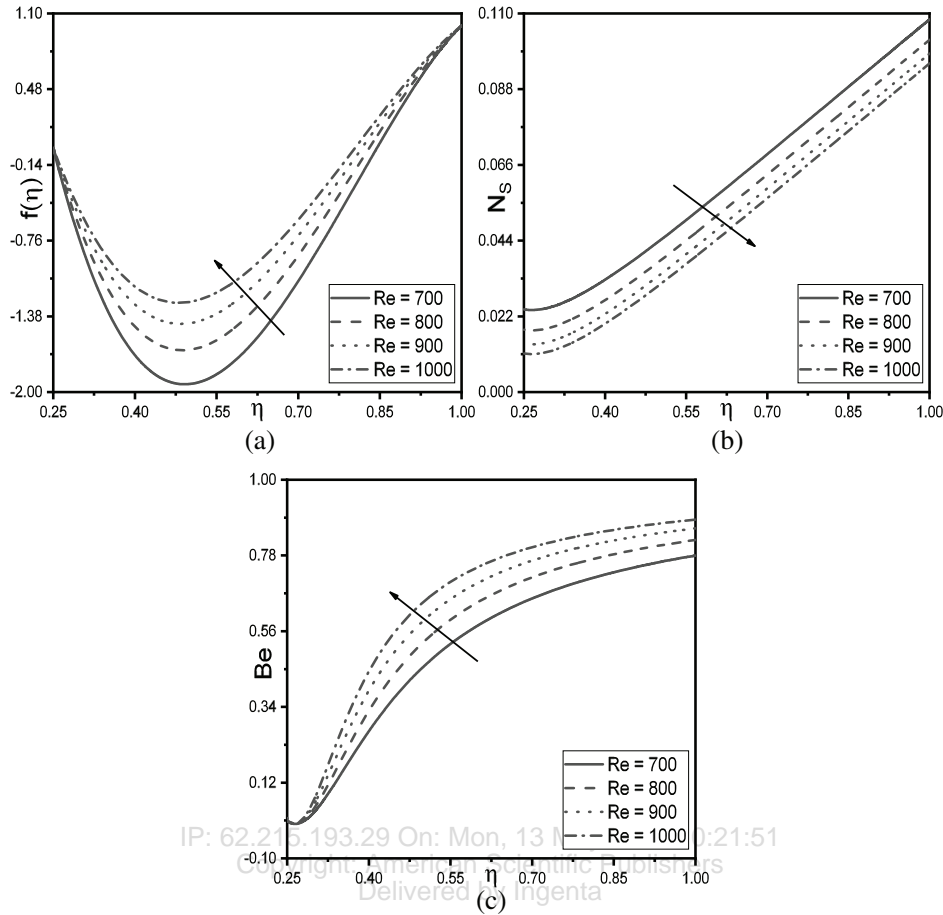


Fig. 2. Influence of Re on (a) f , (b) N_s and (c) Be .

$$\begin{aligned}
 b_{4,r} &= A_3 A_5 Du \eta, & b_{5,r} &= A_3 (A_4 N_b \eta \theta'_r + A_5 Du), \\
 c_{1,r} &= \left(\frac{N_t}{N_b} + Sr \right) \eta, & c_{2,r} &= \frac{N_t}{N_b} + Sr, & c_{3,r} &= \eta \\
 p_r &= \frac{-4}{\Theta_r} (\eta (f_r'' \theta_r - f_r' \theta_r') - f_r \theta_r') + \frac{Gr}{Re} \sqrt{\eta} A_1 \\
 & \left(A_2 \left(\frac{\theta_r^3}{\Theta_r^2} - \frac{2\theta_r^2}{\Theta_r} \right) - N_r \left(\frac{\theta_r^2 \phi_r}{\Theta_r^2} - \frac{2\theta_r \phi_r}{\Theta_r} \right) \right) \\
 & + A_1 P_1 \left(1 - \frac{\theta_r^2}{\Theta_r^2} \right) \\
 q_r &= A_3 A_4 \eta (N_b \theta_r' \phi_r' + N_t \theta_r'^2)
 \end{aligned}$$

We apply the spectral collocation method to iterate the functions using Chebyshev polynomials and Gauss Lobatto collocation points. The Gauss Lobatto collocation points are defined as $\xi_j = \cos(\pi j/N)$, $j = 0, 1, 2, \dots, N$ and the space $[\eta_0, 1]$ is mapped to these collocation points by $\eta = ((1 - \eta_0)\xi + (1 + \eta_0))/2$. Hence the unknown functions are approximated as

$$f_{r+1}(\xi) \approx \sum_{k=0}^N f_{r+1}(\xi_k) T_k(\xi_j),$$

$$\begin{aligned}
 \theta_{r+1}(\xi) &\approx \sum_{k=0}^N \theta_{r+1}(\xi_k) T_k(\xi_j) \quad \& \\
 \phi_{r+1}(\xi) &\approx \sum_{k=0}^N \phi_{r+1}(\xi_k) T_k(\xi_j) \quad (21)
 \end{aligned}$$

where $T_k(\xi) = \cos(k \cos^{-1}(\xi))$ is the Chebyshev polynomial. Furthermore, the derivatives are given by

$$\begin{aligned}
 \frac{d^r f_{r+1}}{d\eta^r} &= \sum_{k=0}^N D_{kj}^r f_{r+1}(\xi_k) \frac{d^r \theta_{r+1}}{d\eta^r} = \sum_{k=0}^N D_{kj}^r \theta_{r+1}(\xi_k) \quad \& \\
 \frac{d^r \phi_{r+1}}{d\eta^r} &= \sum_{k=0}^N D_{kj}^r \phi_{r+1}(\xi_k), \\
 & j = 0, 1, \dots, N \quad (22)
 \end{aligned}$$

Here $D = D/2$ is called Chebyshev spectral matrix of differentiation. We substitute the approximations (4) and the derivatives (4) in (17)–(20) to obtain a matrix equation of the form,

$$\mathcal{A} Y_{r+1} = \mathcal{R}_r, \quad (23)$$

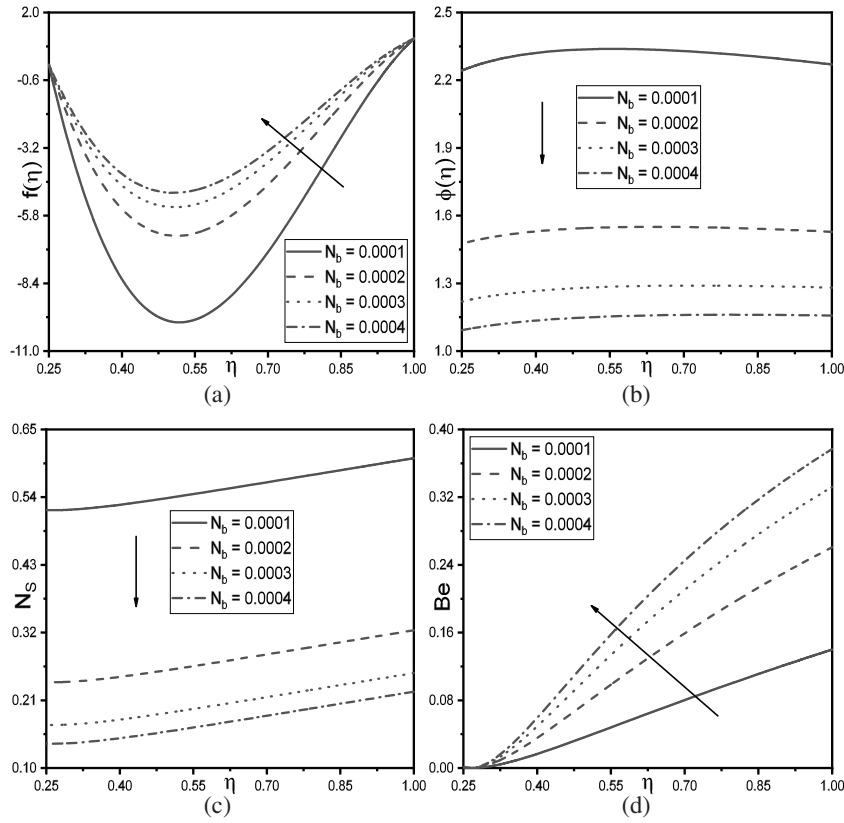


Fig. 3. Influence of N_b on (a) f , (b) ϕ , (c) N_s and (d) Be .

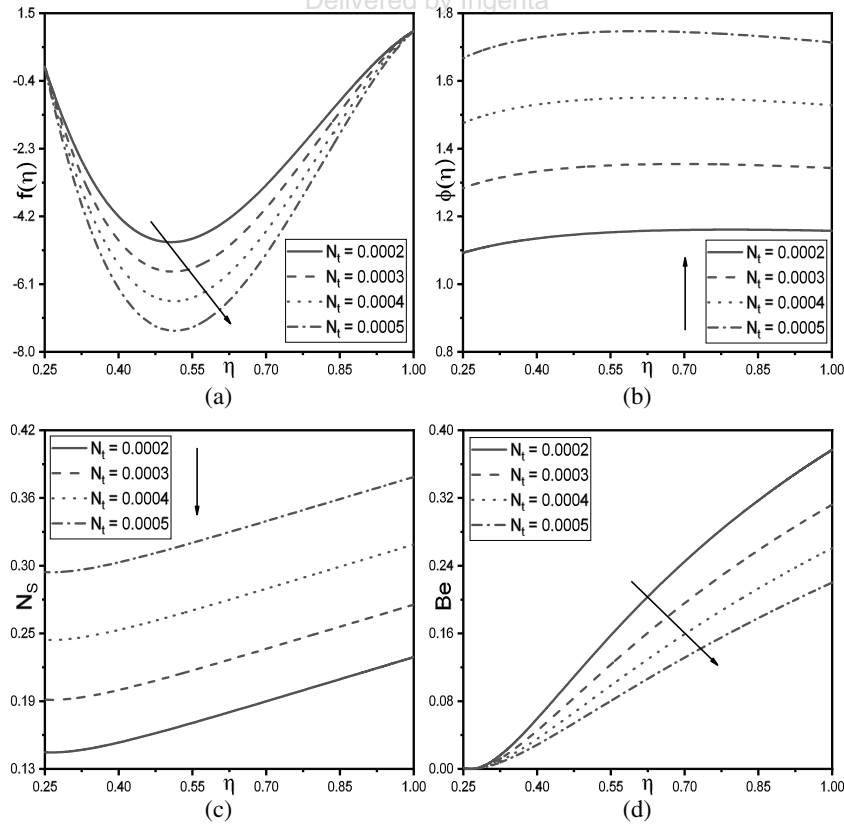


Fig. 4. Influence of N_i on (a) f , (b) ϕ , (c) N_s and (d) Be .

associated with the boundary conditions

$$\left. \begin{aligned}
 f_{r+1}(\xi_0) &= b, \\
 (2D_{00} + A_3 Bi_t) \theta_{r+1}(\xi_0) + 2 \sum_{k=1}^N D_{0k} \theta_{r+1}(\xi_k) \\
 &= A_3 Bi_t (2D_{00} + Bi_c) \phi_{r+1}(\xi_0) + 2 \sum_{k=1}^N D_{0k} \phi_{r+1}(\xi_k) = Bi_c \\
 f_{r+1}(\xi_N) &= 0, \\
 2\sqrt{\eta_0} \sum_{k=0}^{N-1} D_{Nk} \theta_{r+1}(\xi_k) + (2\sqrt{\eta_0} D_{NN} - A_3 Bi_t) \theta_{r+1}(\xi_N) &= 0 \\
 2\sqrt{\eta_0} \sum_{k=0}^{N-1} D_{Nk} \phi_{r+1}(\xi_k) + (2\sqrt{\eta_0} D_{NN} - Bi_c) \phi_{r+1}(\xi_N) &= 0
 \end{aligned} \right\} (24)$$

We choose the initial functions as $f_0 = (\eta - \eta_0)/(1 - \eta_0)$, $\theta_0 = (A_3 Bi_t (\eta - \eta_0) + 2\sqrt{\eta_0}) / (A_3 Bi_t (1 - \eta_0) + 2(1 + \sqrt{\eta_0}))$, $\phi_0 = (Bi_c (\eta - \eta_0) + 2\sqrt{\eta_0}) / (Bi_c (1 - \eta_0) + 2(1 + \sqrt{\eta_0}))$ to satisfy the boundary conditions (20). These initial conditions are iterated to obtain the numerical solution.

5. RESULTS

The matrix equation is solved and the obtained values of velocity, temperature and concentration are depicted graphically in this section by varying the parameter values in the practical range.^{43,44} Since, the Newtonian behaviour water based graphene oxide nanofluid is considered, we take the fixed values of nanoparticle volume fraction and Prandtl number to be $\Phi = 0.01$ and $Pr = 6.5$. The values

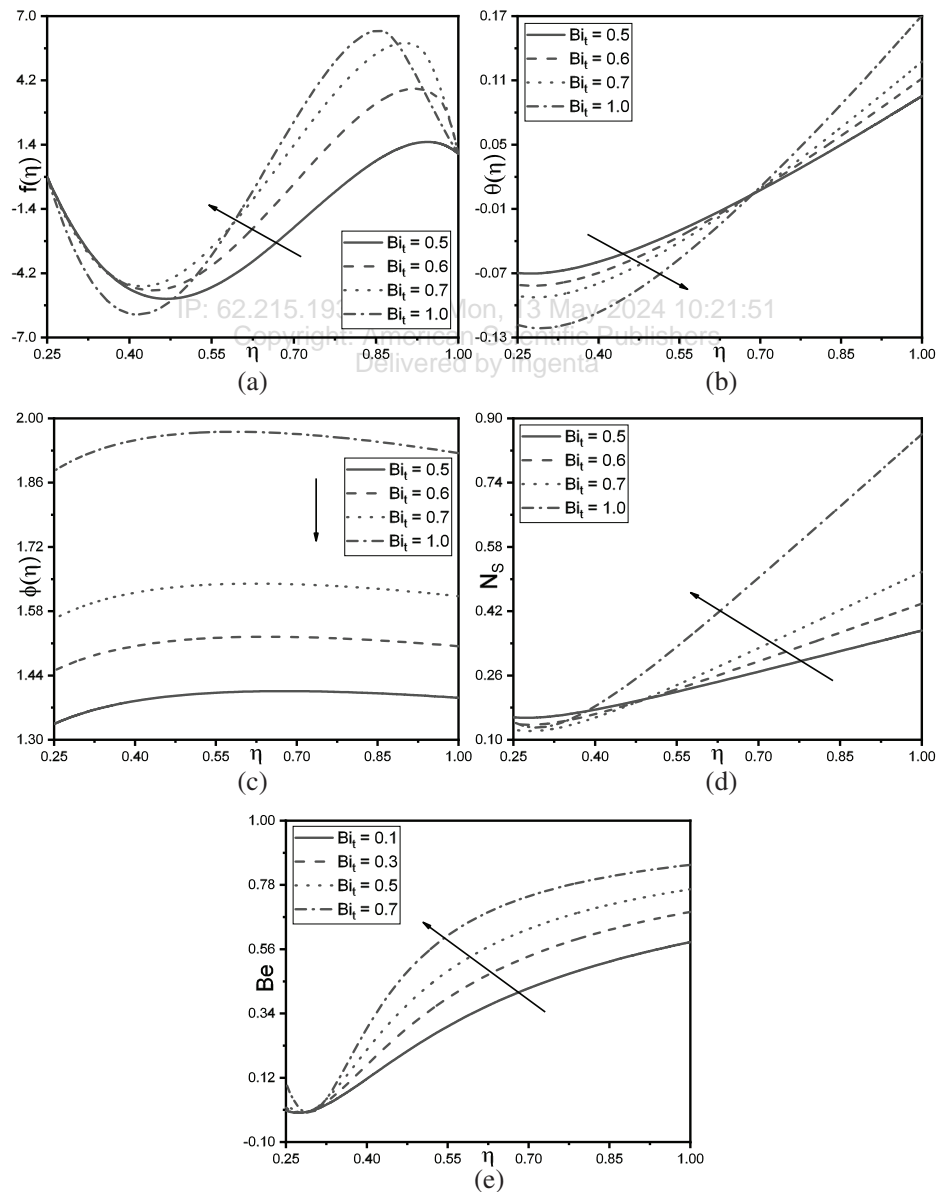


Fig. 5. Influence of Bi_t on (a) f , (b) θ and (c) ϕ , (d) N_s and (e) Be .

of other parameters are chosen as $Bi_t = 0.7$, $Bi_c = 0.8$, $N_b = 2 \times 10^{-4}$, $N_t = 4 \times 10^{-4}$, $Re = 700$, $N_r = 0.2$, $Gr = 2 \times 10^6$, $q_1 = 1$, $\Theta_r = 0.1$, $Du = 0.001$ and $Sr = 0.01$ unless mentioned otherwise. The order of SLM approximation is taken to be $N = 100$ and the convergence of results are obtained at third iteration. The results for the case of $Gr = P_1 = R_d = C_R = 0$, from the present study are compared to the results from Sinha and Chaudhary⁴⁵ in Table II and the values are observed to be in good agreement.

Figure 2 depicts the influence of Re on f , N_S and Be . As the Reynolds number increases, the impacts of viscous forces decrease and the flow velocity increases near the inner cylinder. But near the outer cylinder, the velocity is observed to decrease (Fig. 2(a)). Similarly, the increasing Re values reduces the loss of entropy and hence the entropy number also decreases (Fig. 2(b)). This results in an increase in the Bejan number, suggesting the contribution of fluid friction and mass transfer to the generated entropy (Fig. 2(c)).

The impacts of N_b on f , ϕ , N_S and Be are depicted in Figure 3. There is an increase in velocity near the inner cylinder and decrease near the outer cylinder as N_b increases (Fig. 3(a)). The increase in Brownian motion parameter increases the Brownian motion of the nanoparticles and hence the velocity increases. Also, the Brownian

diffusion causes the nanoparticle concentration to deplete and hence ϕ decreases (Fig. 3(b)) and the diluted fluid moves with greater velocity. Consequently, there is a reduction in the entropy number (Fig. 3(c)), which causes the Bejan number to increase, suggesting the contribution of fluid friction and mass transfer to the generated entropy (Fig. 3(d)).

Figure 4 presents the impacts of N_t on f , ϕ , N_S and Be . The increase in thermophoresis parameter enhances the thermophoresis and the concentrated fluid moves with lesser velocity and hence f decreases (refer Fig. 4(a)). The increase in thermophoresis parameter increases the thermophoretic diffusion of the nanoparticles and hence the nanofluid concentration increases (refer Fig. 4(b)). Consequently, there is a depletion in the entropy number (Fig. 4(c)), which causes the Bejan number to decrease, suggesting the contribution of heat transfer to the generated entropy (Fig. 4(d)).

Figures 5 represents the effects of Bi_t on f , θ , ϕ , N_S and Be . When Bi_t increases, an increase in the velocity is observed, whereas for maximum Bi_t , a shift in the velocity values are obtained sooner because of the higher convection (refer Fig. 5(a)). Whereas, increasing the Bi_t increases the heat transfer coefficient thus increasing the heat transfer from the inner cylinder to the outer cylinder.

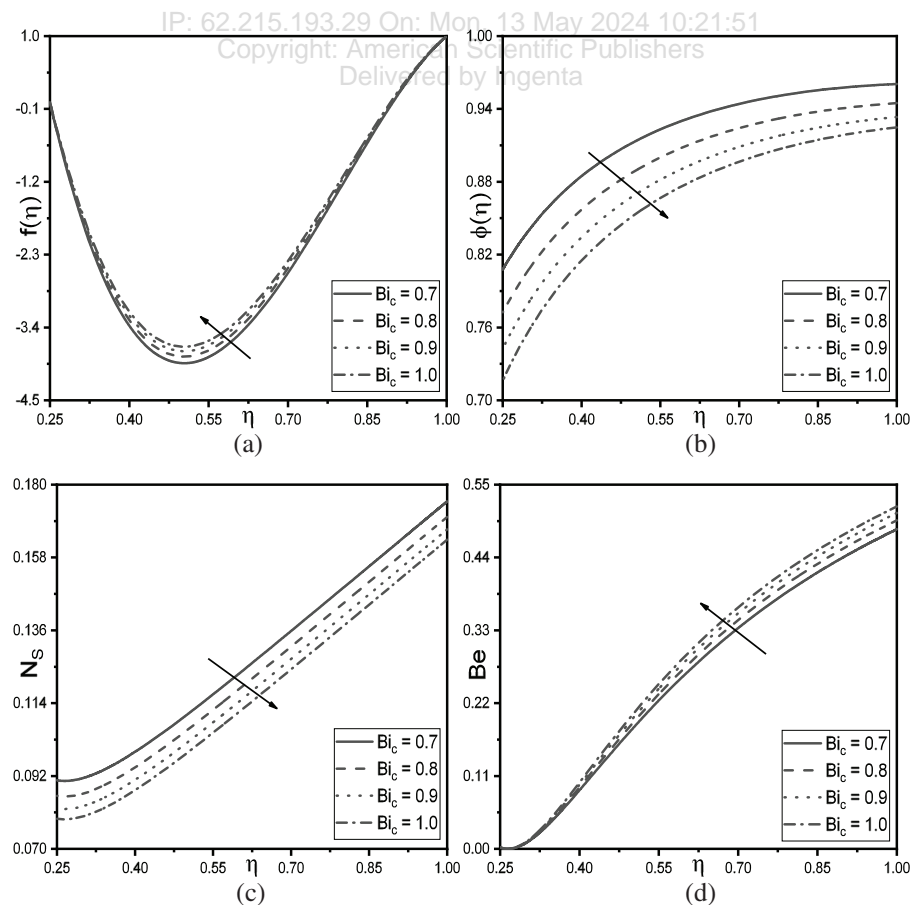


Fig. 6. Influence of Bi_c on (a) f , (b) ϕ , (c) N_S and (d) Be .

Hence there is a rise in the temperature of the nanofluid at the outer cylinder and decrease at the inner cylinder (Fig. 5(b)). Figure 5(c) shows that there is a decrease in the concentration of the nanofluid. From Figure 5(d), it is observed that N_S increases with the values of Bi_i . This is because, the increasing heat transfer coefficient increases the nanofluid temperature and hence N_S increases. This results in an increased Be thus emphasising the dominance of heat transfer on the increased entropy (Fig. 5(e)).

The impacts of Bi_c on f , ϕ , N_S and Be is shown in Figure 6. An increase in Bi_c boosts the mass transfer by enhancing the coefficient of convective mass transfer. This results in an enhanced nanofluid velocity (Fig. 6(a)). The enhanced mass transfer is supposed to cause an increase in concentration values but the concentration profiles decrease because of the variable viscosity (Fig. 6(b)) and the thinner fluid moves with lesser velocity (Fig. 6(a)). Similarly, there is a reduction in N_S (Fig. 6(c)). This results in an increasing Be (Fig. 6(c)). Hence, fluid friction and mass transfer contribute to the entropy in the flow channel.

Figure 7 shows the impacts of Θ_r on f , N_S and Be . As the Θ_r values increase, there is a reduction in velocity profiles (Fig. 7(a)). Whereas, N_S increases with increasing variable viscosity parameter (Fig. 7(b)) and consequently Be decreases (Fig. 7(c)). This implies the irreversibility is

solely responsible for the increased entropy generation is by fluid friction and mass transfer.

The impacts of Soret number on ϕ , N_S and Be is depicted in Figure 8. An increase in the values of Sr implies there is an increase in thermophoretic diffusion which causes an increase in dimensionless concentration (Fig. 8(a)). Likewise, N_S increases with increasing Sr values (Fig. 8(b)) and consequently Be decreases (Fig. 8(c)). This implies the irreversibility is solely responsible for the increased entropy generation is by fluid friction and mass transfer.

Table III presents the values of Nu , Sh and C_f at the surface of the inner cylinder. By definition, Nusselt number is the ratio between convection to conduction at the surface, and at the surface, Nu increases with increasing Bi_i . This implies that the convection at the surface of the cylinder increases with convective heat transfer, because, as the thermal Biot number increases, convective heat transfer increases and the nanoparticles move with higher kinetic energy, thus improving the convective heat transfer at the surface. Similarly, when N_b increases, the values of Sh increases. Thus, Brownian motion parameter enhances the concentration profiles by convection. While, N_t and Sr enhance the diffusion at the surface by respectively enhancing thermophoretic diffusion and chemical reaction.

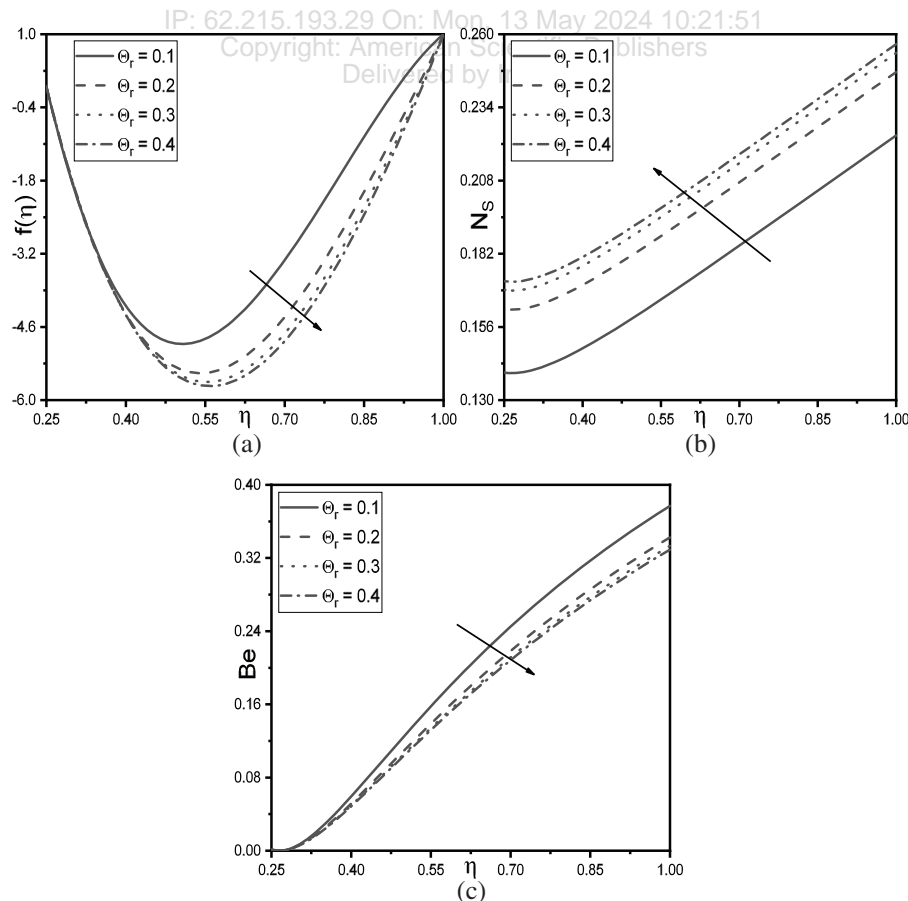


Fig. 7. Influence of Θ_r on (a) f , (b) N_S and (c) Be .

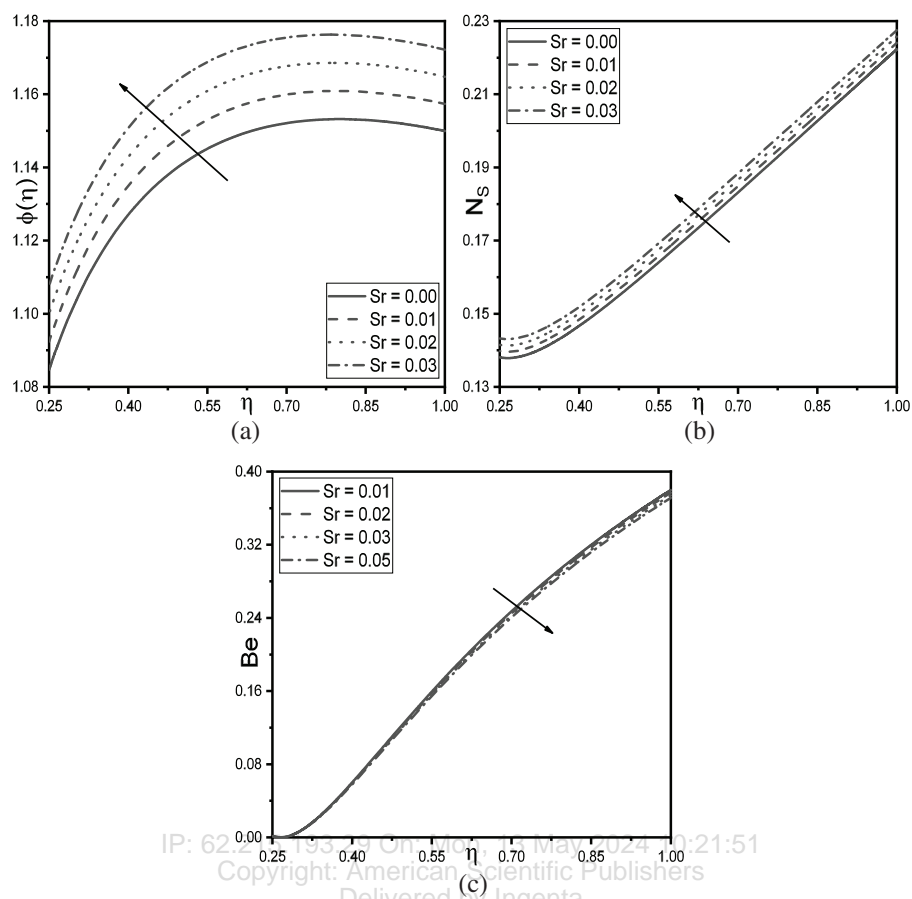


Fig. 8. Influence of Du on (a) ϕ , (b) N_s and (c) Be .

Table III. Nusselt number, Sherwood number and skin friction values.

N_b	N_t	Sr	Θ_r	Bi_t	Bi_c	$-\theta'(\eta_0)$	$-\phi'(\eta_0)$	$C_f Re$
0.0001	0.0002	0.01	0.1	0.3	0.3	0.013907	-0.672776	-172.627418
0.0002	0.0002	0.01	0.1	0.3	0.3	0.013907	-0.442728	-117.462511
0.0003	0.0002	0.01	0.1	0.3	0.3	0.013907	-0.366046	-99.074193
0.0004	0.0002	0.01	0.1	0.3	0.3	0.013907	-0.327704	-89.880028
0.0004	0.0002	0.01	0.1	0.3	0.3	0.013907	-0.327704	-89.880028
0.0004	0.0003	0.01	0.1	0.3	0.3	0.013907	-0.385216	-103.671239
0.0004	0.0004	0.01	0.1	0.3	0.3	0.013907	-0.442728	-117.462441
0.0004	0.0005	0.01	0.1	0.3	0.3	0.013907	-0.500240	-131.253633
0.0004	0.0002	0	0.1	0.3	0.3	0.013907	-0.325404	-89.328377
0.0004	0.0002	0.01	0.1	0.3	0.3	0.013907	-0.327704	-89.880028
0.0004	0.0002	0.02	0.1	0.3	0.3	0.013907	-0.330005	-90.431679
0.0004	0.0002	0.03	0.1	0.3	0.3	0.013907	-0.332305	-90.983331
0.0004	0.0002	0.01	0.1	0.3	0.3	0.013907	-0.327704	-89.880028
0.0004	0.0002	0.01	0.2	0.3	0.3	0.013907	-0.327704	-104.527447
0.0004	0.0002	0.01	0.3	0.3	0.3	0.013907	-0.327704	-109.826100
0.0004	0.0002	0.01	0.4	0.3	0.3	0.013907	-0.327704	-112.545775
0.0004	0.0002	0.01	0.1	0.5	0.3	0.035950	-0.400289	-96.317111
0.0004	0.0002	0.01	0.1	0.6	0.3	0.050001	-0.435092	-94.257305
0.0004	0.0002	0.01	0.1	0.7	0.3	0.065784	-0.468977	-93.599504
0.0004	0.0002	0.01	0.1	1	0.3	0.121761	-0.565600	-107.034625
0.0004	0.0002	0.01	0.1	0.3	0.7	0.013907	-0.565309	-72.314274
0.0004	0.0002	0.01	0.1	0.3	0.8	0.013907	-0.617888	-70.382783
0.0004	0.0002	0.01	0.1	0.3	0.9	0.013907	-0.668105	-68.792922
0.0004	0.0002	0.01	0.1	0.3	1	0.013907	-0.716118	-67.447396

Similarly, the skin friction drag, even if it is very small is impacted by the embedded parameters. Moreover, N_b , Bi_t and Bi_c enhance the skin friction, while, N_t , Sr and Θ_r reduce the skin friction drag at the surface.

6. CONCLUSION

Investigating the flow of water based graphene oxide nanofluids with temperature dependant viscosity in the geometry of concentric cylinders with the impacts of cross-diffusion effects, we infer the following:

- Velocity can be improved by improving the Reynolds number, Brownian motion parameter, thermal and concentration Biot number.
- Heat transfer can be enhanced by enhancing the thermal Biot number.
- Concentration can be increased by amplifying the values of thermophoresis parameter and Soret number which enhances diffusive mass transfer and thermal Biot number which enhances convective mass transfer. Therefore, improving the rate of chemical reaction will improve the mass transfer.
- Skin friction is preferably reduced by enhancing the thermophoresis parameter, Soret number, variable viscosity parameter and thermal Biot number.
- Bejan number is calculated to be $Be < 0.5$ for $0.25 \leq \eta \leq 1$, and hence the generated entropy is predominantly due to fluid friction and combined heat and mass transfer.

As mentioned earlier, the present study is a parametric analysis and the significance widely ranges from the manufacturing of turbines, propulsion systems for spacecrafts, cooling of ships, automobile radiators, cooling towers, shell and tube heat exchangers to the study of blood flow in drug delivery systems. The investigation can be further extended by examining the flow of graphene oxide nanofluid in various other geometries and also by exploring the non-Newtonian behaviour of the nanofluid.

NOMENCLATURE

T	Temperature of the nanofluid
T_a	Temperature of the nanofluid at the inner cylinder
T_b	Temperature of the nanofluid at the outer cylinder
C	Concentration of the nanofluid
C_a	Concentration of the nanofluid at the inner cylinder
C_b	Concentration of the nanofluid at the outer cylinder
u	Radial velocity component
w	Axial velocity component
r	Radial co-ordinate
z	Axial coordinate
g	Acceleration due to gravity
C_p	Specific heat capacity
D_B	Brownian diffusivity
D_T	Thermophoretic diffusivity
h	Heat transfer coefficient

k	Mass transfer coefficient
f	Dimensionless velocity
N_r	Buoyancy ratio
Pr	Prandtl number
Ec	Eckert number
N_b	Brownian diffusion coefficient number
N_t	Thermophoretic diffusion coefficient number
Bi_t	Thermal Biot number
Bi_c	Concentration Biot number
Nu	Nusselt Biot number
Sh	Sherwood number
C_f	Skin friction
Re	Reynolds number
R	Universal gas constant
S_G	Entropy generation rate
N_S	Dimensionless entropy generation number
Sr	Soret number
Du	Dufour number
Θ_r	Variable viscosity parameter
Ω	Angular velocity
ρ	Density
β	Thermal expansion coefficient
κ	Thermal conductivity
μ	Dynamic viscosity
ν	Kinematic viscosity
τ	Heat capacity ratio
Φ	Nanoparticle volume fraction
η	Similarity variable
ψ	Stream function
θ	Dimensionless temperature
ϕ	Dimensionless concentration
χ	Constant parameter
Ω_T	Temperature parameter
Ω_C	Concentration parameter

References and Notes

1. J. Buongiorno, *J. Heat Transfer*. 128, 240 (2006).
2. L. R. Mack and H. C. Hardee, *Int. J. Heat Mass Transf.* 11, 387 (1968).
3. Y. Renardy and D. D. Joseph, *J. Fluid Mech.* 150, 381 (1985).
4. E. Abu-Nada, Z. Masoud, and A. Hijazi, *Int. Commun. Heat Mass Transf.* 35, 657 (2008).
5. Z.-T. Yu, X. Xu, Y.-C. Hu, L.-W. Fan, and K.-F. Cen, *Int. J. Heat Mass Transf.* 55, 1141 (2012).
6. A. Abedini, S. Emadoddin, and T. Armaghani, *Int. J. Numer. Methods Heat Fluid Flow* 29, 1506 (2019).
7. X. Liu, D. Toghraie, M. Hekmatifar, O. A. Akbari, A. Karimipour, and M. Afrand, *J. Therm. Anal. Calorim.* 141, 2095 (2020).
8. S. Gouran, S. Mohsenian, and S. E. Ghasemi, *Alexandria Eng. J.* 61, 3237 (2022).
9. A. H. Pordanjani and S. Aghakhani, *Heat Transf. Eng.* 43, 937 (2022).
10. F. C. Lai and F. A. Kulacki, *Int. J. Heat Mass Transf.* 33, 1028 (1990).
11. M. Y. Malik, A. Hussain, and S. Nadeem, *Sci. Iran.* 20, 313 (2013).
12. A. Hussain and A. Ullah, *Alexandria Eng. J.* 55, 3073 (2016).
13. K. Kaladhar, C. RamReddy, D. Srinivasacharya, and T. Pradeepa, *Math. Sci.* 10, 139 (2016).

14. S. Darbhasayanam and J. Pashikanti, *Model. Meas. Control B.* 87, 7 (2018).
15. D. Srinivasacharya and P. Jagadeeshwar, *Math. Sci.* 13, 201 (2019).
16. M. Irfan, M. A. Farooq, and T. Iqra, *Front. Phys.* 8 (2020), DOI: 10.3389/fphy.2020.00066.
17. E. R. G. Eckert and R. M. Drake Jr., *Analysis of Heat and Mass Transfer* (1972).
18. D. Srinivasacharya, R. Bhuvanavijaya, and B. Mallikarjuna, *Procedia Eng.* 127, 271 (2015).
19. R. A. Shah, A. Khan, and M. Shuaib, *Heat Transf. Res.* 49, 1103 (2018).
20. A. Rehman, Z. Salleh, and T. Gul, *J. Nanofluids.* 8, 1661 (2019).
21. D. Srinivasacharya, P. Jagadeeshwar, D. Srinivasacharya, and P. Jagadeeshwar, *J. Nanofluids.* 8, 1592 (2019).
22. J. A. Gbadeyan, E. O. Titiloye, and A. T. Adeosun, *Heliyon* 6, e03076 (2020).
23. R. Sharma, S. M. Hussain, C. S. K. Raju, G. S. Seth, and A. J. Chamkha, *Chinese J. Phys.* 68, 671 (2020).
24. B. Souayeh, K. G. Kumar, M. G. Reddy, S. Rani, N. Hdhiri, H. Alfannakh, and M. Rahimi-Gorji, *J. Mol. Liq.* 290, 111223 (2019).
25. M. G. Reddy, M. S. Rani, K. G. Kumar, B. C. Prasannakumar, and H. J. Lokesh, *Phys. A: Stat. Mech. Appl.* 551, 123975 (2020).
26. M. G. Reddy, N. Kumar, B. C. Prasannakumara, N. G. Rudraswamy, and K. G. Kumar, *Commun. Theor. Phys.* 73, 045002 (2021).
27. K. G. Kumar, E. H. B. Hani, M. E. H. Assad, M. Rahimi-Gorji, and S. Nadeem, *Microsyst. Technol.* 27, 97 (2021).
28. K. Ganesh Kumar, *Eur. Phys. J. Plus* 137, 1 (2022).
29. L. S. Naik, D. G. Prakasha, M. V. V. N. L. Sudharani, and K. G. Kumar, *Int. J. Mod. Phys. B.* 2450134 (2023).
30. D. G. Prakasha, M. V. V. N. L. Sudharani, K. G. Kumar, E. M. Elsaid, and M. R. Eid, *J. Therm. Anal.* 148, 6197 (2023).
31. M. V. V. N. L. Sudharani, D. G. Prakasha, K. G. Kumar, and A. J. Chamkha, *Eur. Phys. J. Plus* 138, 257 (2023).
32. S. S. Ghadikolaie, K. Hosseinzadeh, M. Hatami, D. D. Ganji, and M. Armin, *J. Mol. Liq.* 263, 10 (2018).
33. Y.-M. Chu, K. S. Nisar, U. Khan, H. Daei Kasmaei, M. Malaver, A. Zaib, and I. Khan, *Water* 12, 1723 (2020).
34. D. R. Lide and H. V. Kehiaian, *CRC Handbook of Thermophysical and Thermochemical Data.* CRC Press (2020).
35. K. Al-Sankoor, H. Al-Gayyim, S. Al-Musaedi, Z. Asadi, and D. D. Ganji, *Case Stud. Therm. Eng.* 27, 101236 (2021).
36. T. Gul, M. Z. Ullah, A. K. Alzahrani, and I. S. Amiri, *IEEE Access* 7, 102345 (2019).
37. 11. K. Elsaid, M. A. Abdelkareem, H. M. Maghrabie, E. T. Sayed, T. Wilberforce, A. Baroutaji, and A. G. Olabi, *Int. J. Thermofluids* 10, 100073 (2021).
38. A. Bejan, *J. Appl. Phys.* 79, 1191 (1996).
39. A. Bejan and J. Kestin, *J. Appl. Mech.* 50, 475 (1983).
40. S. Paoletti, F. Rispoli, and E. Sciubba, *Calculation of Exergetic Losses in Compact Heat Exchanger Passages*, ASME AES. pp. 21–29 (1989).
41. R. E. Bellman and R. E. Kalaba, *Am. Math. Mon.* 74, 1157 (1967).
42. C. Canuto, K. Taira, et al., *Spectral Methods*, Berlin, Heidelberg, Springer Berlin Heidelberg.
43. M. S. Malashetty, J. C. Umavathi, and J. Prathap Kumar, *Heat Mass Transf.* 37, 259 (2001).
44. A. Behseresht, A. Noghrehabadi, and M. Ghalambaz, *Chem. Eng. Res. Des.* 92, 447 (2014).
45. K. D. Sinha and R. C. Chaudhary, *Proc. Nat. Inst. Sci. India* 32, 81 (1966).

IP: 62.215.193.29 On: Mon, 13 May 2024 10:21:51
 Copyright: American Scientific Publishers
 Delivered by Ingenta